Report

Design of the NIPR trajectory model

Yoshihiro Tomikawa[1]* and Kaoru Sato[1,2]

[1]*National Institute of Polar Research, Kaga 1-chome, Itabashi-ku, Tokyo 173-8515*
[2]*Now at Department of Earth and Planetary Science, The University of Tokyo, Tokyo 113-0033*
Corresponding author. E-mail: tomikawa@nipr.ac.jp

Abstract: Kinematic and isentropic trajectory models developed at the National Institute of Polar Research (NIPR) are compared with METEX developed at the Center for Global Environmental Research, National Institute for Environmental Studies (CGER/NIES). The NIPR model shows good agreement with METEX both in the kinematic and isentropic trajectories. An intercomparison between the trajectories computed with different datasets is also performed using the NIPR model, and shows that the accuracy of the trajectory is far more sensitive to the difference of the dataset used than to the difference of trajectory model.

key words: trajectory, Lagrangian, METEX

1. Introduction

Trajectory models have been developed at many institutes in the last several decades. Most of the recent trajectory models are classified into two categories based on the method used to determine the vertical position of an air parcel. One is the model that advects the air parcel with the vertical wind. The other is the model that advects the air parcel on a constant potential temperature surface. The former is called a kinematic trajectory model, and the latter is called an isentropic trajectory model.

Air parcel trajectories have been commonly used in order to identify the origin of air parcels. Danielsen (1968) showed that the air parcels in the subtropical tropopause folding had a stratospheric origin, using their isentropic trajectories. The recent increase of interest in the emission inventory of polluted air (Lelieveld *et al.*, 2001) has promoted the usage of trajectories. In the Match experiment using ozonesonde (von der Gathen *et al.*, 1995) or satellite (Terao *et al.*, 2002) data, the ozone loss rate along the trajectories is estimated under the assumption that the air parcels observed at two different locations are identical. In these analyses, each trajectory represents an air parcel having a finite volume, and it is assumed that the trajectory keeps on representing the same air parcel during the advection for several days.

Several kinds of dynamical and chemical tracers such as Ertel's potential vorticity and nitrous oxide (N_2O) are conserved following the air parcel motion. By combining

the air parcel trajectories with any conserved quantities, small-scale distributions of these conserved quantities, which cannot be directly observed, can be obtained. Waugh and Plumb (1994) and Norton (1994) computed forward isentropic trajectories of the air parcels placed on the contours of the conserved quantities such as Ertel's potential vorticity and N_2O mixing ratio, and reproduced the small-scale features of these contours in several days (*i.e.*, contour advection with surgery). Small-scale distributions of these conserved quantities at a certain time can also be obtained using backward isentropic trajectories of the air parcels placed on a regular grid (*i.e.*, reverse domain filling, Sutton *et al*., 1994; Tomikawa *et al*., 2002). A similar method is used for the estimate of stratosphere-troposphere exchange (Dethof *et al*., 1999, 2000; Vaughan and Timmis, 1998).

These trajectory-based methods are applied over a short time scale such as several days. As the time period of trajectory calculation becomes longer, the identity of the air parcel is lost because of the uncertainty of trajectory calculation and the diffusive nature of the atmosphere. On the other hand, statistical information on the air parcels is still significant after a long time, even several years. Kida (1983) computed forward kinematic trajectories of the air parcels arranged at the tropical tropopause for several years, and described the characteristics of the Brewer-Dobson circulation in the stratosphere using the probability distribution functions (PDFs) of the elapsed time (*i.e.*, age) in which the air parcel traveled from the tropical tropopause to the specified region. These PDFs of air parcel age are called age spectra, and are used in many studies of passive tracer transport (Waugh and Hall, 2002, and references therein).

The trajectory-based methods mentioned above do not consider what happens in the air parcel during the advection. However, the growing interest in the ozone hole in the last two decades has created a need for information on chemical reactions along the trajectories. Reid *et al*. (1998) combined a chemical box model with diabatic trajectories, and estimated an ozone loss rate along the trajectories.

Information on trajectories is often used in making observations. In the ozonesonde Match experiment to estimate the ozone loss rate, forward trajectories were used to determine the time of the next ozonesonde release (Rex *et al*., 2002). The flight routes of observational aircraft are often determined based on the results of forward trajectories (Jacob *et al*., 2003).

Air parcel trajectories are used also in studies of, for example, warm conveyor belts (*e.g*., Stohl, 2001), the tropical tropopause layer (*e.g*., Hatsushika and Yamazaki, 2003), and so on. Based on the increasing demand for a trajectory model, the authors developed kinematic and isentropic trajectory models at the National Institute of Polar Research (NIPR). A prototype of the NIPR isentropic trajectory model was developed by Sato and Dunkerton (2002) to examine the origin of inertially unstable air parcels observed in middle latitudes. Although some papers using the NIPR trajectory models have already been published (Fujiwara *et al*., 2003; Hara *et al*., 2003; Koike *et al*., 2003; Oshima *et al*., 2004; Suzuki *et al*., 2004; Yamanouchi *et al*., 2005), these models have not yet been evaluated. The purpose of this paper is to compare these trajectory models with METEX (Zeng *et al*., 2003), which is a free trajectory model developed at the Center for Global Environmental Research, National Institute for Environmental Studies (CGER/NIES), and to demonstrate the validity of the NIPR

trajectory models. An intercomparison between the trajectories computed with three different datasets is also performed.

2.   Description of the trajectory models

The kinematic and isentropic trajectory models were recently developed at NIPR. These models can be applied to almost any kind of gridded dataset on any Linux/Unix platform. An air parcel given at a certain time is advected by three- and two-dimensional wind fields in kinematic and isentropic trajectory models, respectively. A fourth-order Runge-Kutta scheme is used for time integration. Wind fields provided by any operational analysis are interpolated in time using cubic spline functions, linearly in longitude and latitude, and linearly in the vertical with respect to log pressure height and potential temperature for kinematic and isentropic trajectories, respectively. Although the time step is set at 60 min by default, it can be changed. The main features of the trajectory models are summarized in Table 1.

The kinematic and isentropic trajectories calculated with the NIPR trajectory models are compared to those calculated with METEX (Zeng *et al*., 2003) developed at CGER/NIES. METEX is used instead of other popular trajectory models such as the HYSPLIT4 of NOAA (Draxler and Hess, 1997) and FLEXTRA of the University of Munich (Stohl, 1999), because they cannot specify the initial levels of trajectories with potential temperature or pressure, whereas METEX can. The validity of METEX was confirmed by comparison with other trajectory models developed at NIES in the past (Zeng *et al*., 2003).

The main features of METEX are given in Table 1. Although METEX uses a time integration scheme different from that of the NIPR model, the discrepancy resulting from the difference of time integration scheme is insignificant (Draxler and Hess, 1997; Zeng *et al*., 2003). A time step in METEX is determined based on the Courant-Friedrichs-Lewy (CFL) criterion and varies with latitude and horizontal wind velocity. Since the grid interval is smaller in the polar region than in lower latitude, the time step

Table 1.   Summary of the main features of the NIPR trajectory models and METEX.

Model	NIPR		METEX	
	Kinematic	Isentropic	Kinematic	Isentropic
Horizontal coordinates	Longitude/Latitude			
Vertical coordinates	Pressure	Potential temperature	Pressure	Potential temperature
Integration scheme	4th-order Runge-Kutta		Petterssen's (1940) scheme	
Time step	60 min		Flexible, < 60 min	
Horizontal interpolation	Bilinear			
Vertical interpolation	Linear with log pressure		Linear with geopotential height	
Time interpolation	Cubic spline		Linear	

becomes short in the polar region. A difference between the NIPR model and METEX, which is not mentioned in Table 1, is the treatment of trajectories in the polar region. In order for the latitude of an air parcel to not exceed $90°$, a coordinate transformation between longitude-latitude coordinates and Cartesian coordinates centered at the pole is performed in METEX when the air parcel approaches the South or North Pole ($>87.5°$). In the NIPR model, the latitude is turned back and the longitude is rotated by $180°$ when an air parcel passes over the South or North Pole. These two differences can cause a large discrepancy of trajectories in the polar region. This issue is examined in Section 4.1.

3. Data and method

3.1. Data

Three kinds of datasets in July 1998 are used for the trajectory calculations. The National Centers for Environmental Prediction (NCEP)/National Center for Atmospheric Research (NCAR) Reanalysis 1 data were provided by the NOAA-CIRES Climate Diagnostics Center through their web site at http://www.cdc.noaa.gov/ (Kalnay *et al*., 1996). The European Centre for Medium-Range Weather Forecasts (ECMWF) operational analysis and the ECMWF 40-year Re-analysis (ERA40) data were provided by ECMWF. The ERA40 data can be freely obtained from their web site at http://www.ecmwf.int/ (ECMWF, 2002). The period of July 1998 was chosen because the polar-night jet in the southern hemisphere has a stronger zonal wind than that in the northern hemisphere and a larger difference of trajectories can be formed. The main features of these datasets such as horizontal resolution and available pressure levels are summarized in Table 2. Although there are a few differences of available pressure levels, horizontal and time resolutions are common to all three datasets.

Table 2.   Summary of the data sets used for trajectory calculations. *T, U, V, W, and G denote the temperature, zonal and meridional winds, omega velocity, and geopotential (height), respectively. The NCEP/NCAR Reanalysis omega velocity data are available only between 1000 and 100 hPa (i.e., 12 levels).*

Data set	NCEP/NCAR Reanalysis 1	ECMWF operational analysis	ECMWF 40-year Re-analysis
Period	July 1–31, 1998 (00, 06, 12, 18 UTC)		
Horizontal grid	$2.5°$ longitude $\times 2.5°$ latitude		
Pressure level	17 (1000, 925, 850, 700, 600, 500, 400, 300, 250, 200, 150, 100, 70, 50, 30, 20, 10 hPa)	15 (1000, 925, 850, 700, 500, 400, 300, 250, 200, 150, 100, 70, 50, 30, 10 hPa)	23 (1000, 925, 850, 775, 700, 600, 500, 400, 300, 250, 200, 150, 100, 70, 50, 30, 20, 10, 7, 5, 3, 2, 1 hPa)
Variable	T, U, V, W, G		

3.2. Intercomparison method

Forward and backward trajectories starting at 0000 UTC on July 10 and 20, 1998 are computed for 72 h. Trajectory periods longer than 72 h are usually used in isentropic trajectories. However, as the trajectory period becomes longer, a discrepancy between two groups of trajectories, which have the same initial positions but are computed with different models or different datasets, begins to result from the difference of air parcel positions rather than the difference of trajectory models and used datasets. In order to focus on the effects of different models and datasets, different groups of trajectories up to 72 h travel time are compared in this paper. Air parcels are arranged every 30° in longitude and every 10° in latitude from 80°S to 80°N. Kinematic trajectories start from 15 pressure levels between 200 and 900 hPa every 50 hPa in order for the air parcel to not rise above 100 hPa, which is the highest level of the omega velocity data of the NCEP/NCAR reanalysis 1. Isentropic trajectories are computed on 8 isentropic surfaces between 350 and 700 K every 50 K. The 700-K isentropic surface is close to the 10-hPa pressure level around the winter pole. Thus 20240 [= 12 (longitudes) × 17 (latitudes) × 15 (pressure levels) × 2 (forward and backward) × 2 (June 10 and 20)] kinematic and 6528 [= 12 × 17 × 8 (isentropic levels) × 2 × 2] isentropic trajectories are computed for four combinations of model and dataset (NIPR/NCEP, METEX/NCEP, NIPR/ECMWF, and NIPR/ERA40). When an air parcel is removed by boundary checking in METEX, it is not included in the comparison.

For intercomparison between different trajectory models or different datasets, absolute horizontal (AHTD) and vertical (AVTD) transport deviations are defined as (*cf.*, Knudsen and Carver, 1994)

$$\text{AHTD}(t) = \frac{1}{N}\sum_{n=1}^{N}\text{HTD}(X(n,t), Y(n,t); x(n,t), y(n,t)), \qquad (1)$$

$$\text{HTD}(X(n,t), Y(n,t); x(n,t), y(n,t))$$
$$= a\cos^{-1}[\cos(X(n,t)-x(n,t))\cos Y(n,t)\cos y(n,t) + \sin Y(n,t)\sin y(n,t)],$$

$$\text{AVTD}(t) = \frac{1}{N}\sum_{n=1}^{N}|Z(n,t)-z(n,t)|, \qquad (2)$$

where HTD is the horizontal travel distance, N is the total number of trajectories, a is the earth's radius, and (X, Y, Z) and (x, y, z) are locations (longitude, latitude, and geopotential height, respectively) of reference and compared trajectories, respectively, which are functions of parcel number (n) and travel time (t). In addition, relative horizontal (RHTD) and vertical (RVTD) transport deviations, which are horizontal and vertical distances between two trajectories relative to their respective travel distances, are defined as

$$\text{LH}(n,t) = \frac{1}{2}\sum_{i=2}^{N_t}[\text{HTD}(X(n,t_i), Y(n,t_i); X(n,t_{i-1}), Y(n,t_{i-1}))$$
$$+ \text{HTD}(x(n,t_i), y(n,t_i); x(n,t_{i-1}), y(n,t_{i-1}))],$$

$$\text{RHTD}(t) = \frac{1}{N}\sum_{n=1}^{N}\frac{\text{HTD}(X(n,t), Y(n,t); x(n,t), y(n,t))}{\text{LH}(n,t)}, \qquad (3)$$

$$\mathbf{LV}(n, t) = \frac{1}{2} \sum_{i=2}^{N_t} [\,|\mathbf{Z}(n, t_i) - \mathbf{Z}(n, t_{i-1})\,| + |z(n, t_i) - z(n, t_{i-1})\,|\,],$$

$$\mathbf{RVTD}(t) = \frac{1}{N} \sum_{n=1}^{N} \frac{|\mathbf{Z}(n, t) - z(n, t)\,|}{\mathbf{LV}(n, t)}, \tag{4}$$

where t_i is the ith time step and N_t is the total number of time steps.

Since the zonal wind velocity depends largely on latitude rather than longitude, the travel distances of trajectories also depend on latitude. When there is a large difference between the travel distances of trajectories, an AHTD is not a good indicator of discrepancy between two groups of trajectories. In order to avoid such a deficiency, all the trajectories are divided into five latitude regions based on their initial latitudes: Winter Pole (W. P.) from 80°S to 60°S, Winter Midlatitude (W. M.) from 50°S to 30°S, Equator (Eq.) from 20°S to 20°N, Summer Midlatitude (S. M.) from 30°N to 50°N, and Summer Pole (S. P.) from 60°N to 80°N.

4. Results

4.1. NIPR/NCEP vs. METEX/NCEP

One example of forward and backward kinematic trajectories calculated with the NIPR model and METEX, starting from 180°E, 30°N at 500 hPa at 0000 UTC on July 10, 1998, is shown in Fig. 1. For comparison, trajectories starting from the same position at the same time were computed with HYSPLIT4 (http://www.arl.noaa.gov/
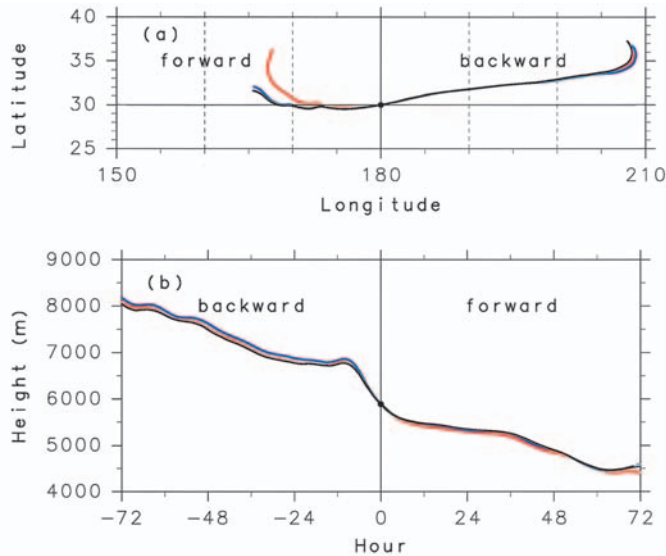

Fig. 1. *(a) Horizontal map and (b) time change of heights of the forward and backward kinematic trajectories calculated with the NIPR model (blue), METEX (red), and HYSPLIT4 (black), starting from 180°E, 30°N at 500 hPa at 0000 UTC on July 10, 1998. Closed circles represent the initial positions of the trajectories.*

ready/hysplit4.html) using the NCEP/NCAR Reanalysis 1 data and are shown in Fig.
1.   The initial vertical position in HYSPLIT4 was specified by the height closest to the
500-hPa pressure level.   Although the height in HYSPLIT4 is not given as a geopo-
tential height but as a height above model ground level, these are almost equivalent over
the ocean.   Three backward trajectories show good agreement both in the horizontal
and vertical positions.   For the forward trajectories, the NIPR trajectory shows better
agreement with the HYSPLIT4 trajectory than with the METEX trajectory.   How-
ever, since the discrepancy between the NIPR and METEX trajectories varies on a
case-by-case basis, the NIPR and METEX trajectories are hereafter compared with each
other using AHTD, RHTD, AVTD, and RVTD, as defined in the previous section.
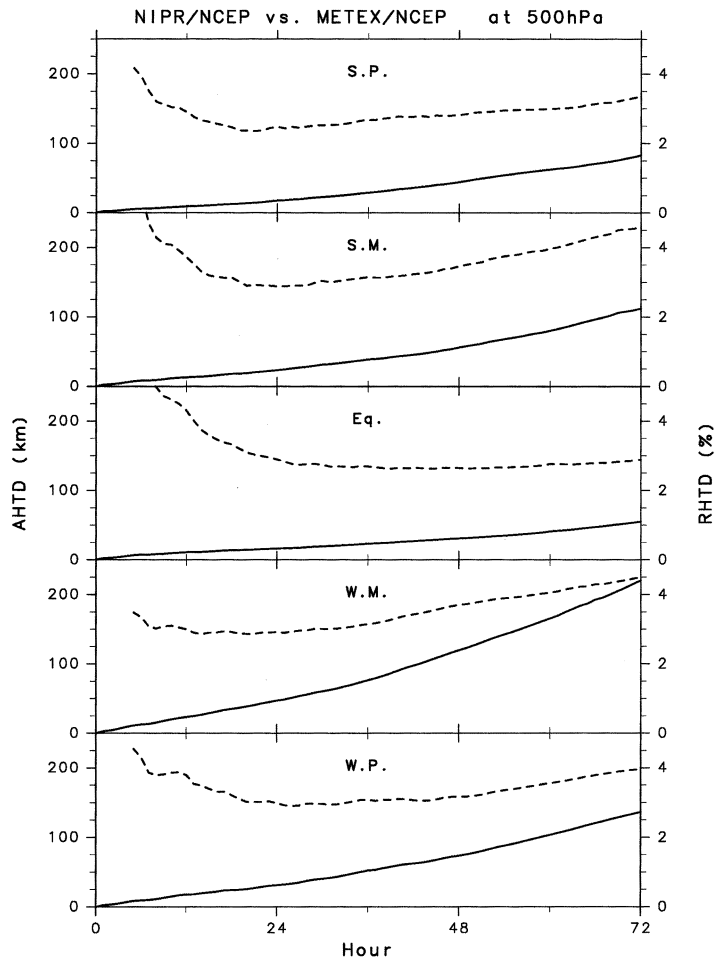   Figure 2 shows the temporal variations of AHTDs and RHTDs for kinematic

Fig. 2.   AHTDs (solid) and RHTDs (dashed) for kinematic trajectories starting at 500 hPa, re-
         sulting from NIPR/NCEP vs. METEX/NCEP in five latitude regions, as a function of
         trajectory period.

trajectories starting at 500 hPa, resulting from NIPR/NCEP *vs.* METEX/NCEP in five latitude regions. The first four hours of the RHTDs are not drawn because the RHTDs were highly variable in that period. Since the subtropical jet in W. M. (Winter Mid-latitude) is strong, the AHTD in W. M. is largest. However, even in W. M. the AHTD is about 200 km at 72 h, which is comparable to or smaller than one grid spacing (200–300 km). The dependence of RHTDs on latitude is small, and the RHTDs at 72 h are 3–5% in all latitude regions. Although it looks like the AHTDs increase almost linearly with time, the increase of the AHTDs is larger in the last 24 h than in the first 24 h. As noted in the previous section, while the discrepancy between the two groups of trajectories starting from the same positions initially results from the difference of the trajectory models such as interpolation method and time integration scheme, this discrepancy results more from the difference of air parcel positions later. Thus the larger increase of the AHTDs in the last 24 hours implies that the AHTDs are more sensitive to the difference of air parcel positions than to the difference of the trajectory models. In contrast, the RHTDs are minimized at 12–36 h. It is considered that the large RHTDs in the first several hours are due to some extremely large RHTDs resulting from small travel distances (not shown). After the RHTDs leveled off at a certain value (*i.e.*, minimum RHTDs), the RHTDs began to increase because the rate of increase of the AHTDs increases with time. These features of AHTDs and RHTDs have been observed in previous studies (*e.g.*, Stohl *et al.*, 1995).

Figure 3 shows the temporal variations of AVTDs and RVTDs for kinematic trajectories starting at 500 hPa, resulting from NIPR/NCEP *vs.* METEX/NCEP in five latitude regions. The AVTDs and RVTDs at 72 h are 100–200 m and 4–8% in all latitude regions, respectively. The largest increase of the AVTDs is observed in the first several hours, unlike the AHTDs. This is due to the larger interpolation errors of vertical velocity than those of zonal and meridional velocities, caused by the high-frequency and small-scale variability of the vertical velocity (Stohl *et al.*, 1995). Since the horizontal and vertical interpolation methods in the NIPR model are almost identical with those in METEX, the difference in the temporal interpolation method (*i.e.*, cubic spline for NIPR and linear for METEX) is considered responsible for the largest increase of the AVTDs in the first several hours. The reason why the RVTDs are larger than the RHTDs can also be explained in the same way. The RVTDs are not minimized at 12–36 h, unlike the RHTDs. This feature has also been seen in previous studies using RVTD (*e.g.*, Stohl *et al.*, 1995), suggesting that interpolation errors of vertical velocity are more critical for the vertical motion of air parcels than the difference of air parcel positions.

Figure 4 shows the AHTDs and RHTDs at 72 h for kinematic trajectories resulting from NIPR/NCEP *vs.* METEX/NCEP in five latitude regions as a function of initial pressure. Although the AHTDs and RHTDs show slight dependence on the initial pressure and latitude region, the AHTDs and RHTDs are up to 200 km and 5%, respectively. Figure 5 shows the AVTDs and RVTDs at 72 h for kinematic trajectories resulting from NIPR/NCEP *vs.* METEX/NCEP in five latitude regions as a function of initial pressure. The AVTDs and RVTDs are up to 200 m and 10%, respectively, in all initial pressures and latitude regions.

Figure 6 shows the AHTDs and RHTDs at 72 h for isentropic trajectories resulting
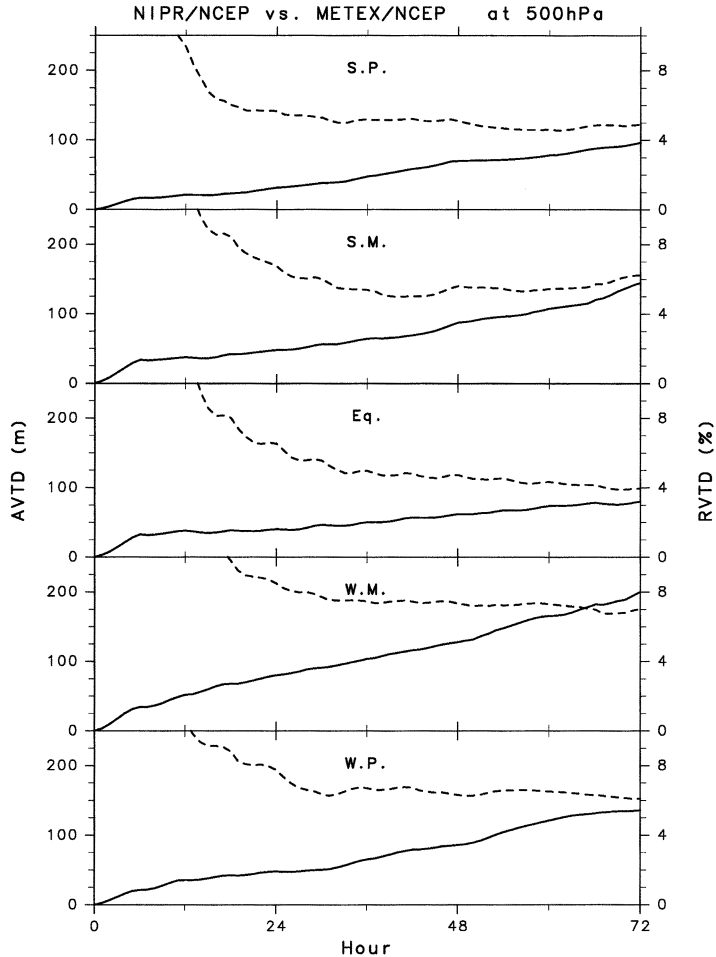
Fig. 3.   *The same as Fig. 2 but for AVTDs (solid) and RVTDs (dashed).*

from NIPR/NCEP *vs.* METEX/NCEP in five latitude regions as a function of potential temperature.   Both AHTDs and RHTDs for isentropic trajectories are smaller than those for kinematic trajectories.   The better agreement between NIPR/NCEP and METEX/NCEP for isentropic trajectories is probably attributable to the lack of vertical advection in isentropic trajectories.   However, this feature just shows the smaller dependence of isentropic trajectories on the difference of trajectory models, and does not mean that the isentropic trajectories are more accurate and realistic than the kinematic trajectories.   When the assumption of adiabatic motion for isentropic trajectories is inappropriate, the isentropic trajectories become unrealistic compared to the kinematic trajectories.

Figures 7a and 7b show the isentropic trajectories at 500 K, which passed over the regions poleward of 87.5°S and 87.5°N, respectively.   The trajectories calculated with the NIPR model show good agreement with those calculated with METEX even after
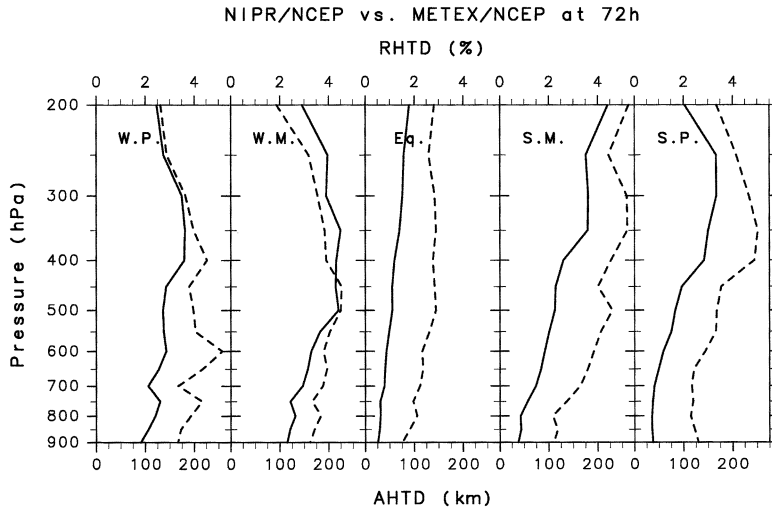
NIPR/NCEP vs. METEX/NCEP at 72h

RHTD (%)

Fig. 4.   AHTDs (solid) and RHTDs (dashed) at 72 h for kinematic trajectories resulting from
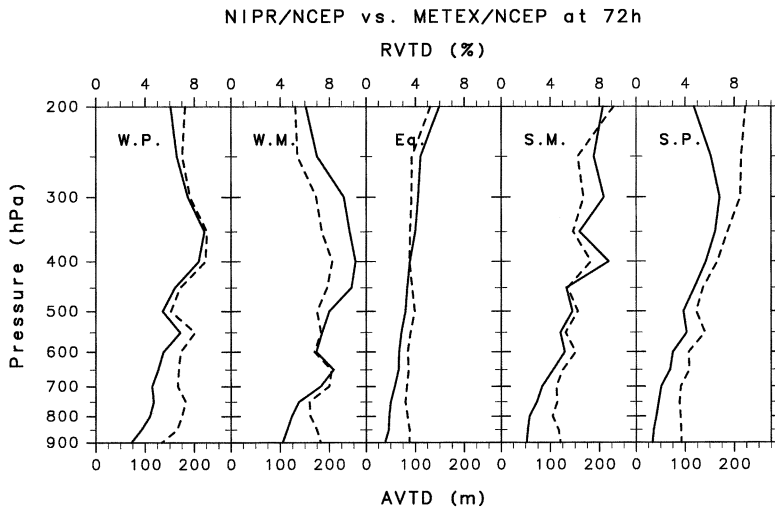NIPR/NCEP vs. METEX/NCEP in five latitude regions as a function of initial pressure.

NIPR/NCEP vs. METEX/NCEP at 72h

RVTD (%)

Fig. 5.   AVTDs (solid) and RVTDs (dashed) at 72 h for kinematic trajectories resulting from
NIPR/NCEP vs. METEX/NCEP in five latitude regions as a function of initial pressure.

passing near the South or North Pole.   As described in the Appendix, the difference
between the trajectories due to the coordinate transformation in the polar region is small
for $u \leq 10\,\mathrm{m\,s^{-1}}$ and $v = 10\,\mathrm{m\,s^{-1}}$.   Since the horizontal advection speed of the tra-
jectories shown in Fig. 7 is at most $10\,\mathrm{m\,s^{-1}}$, the effect of coordinate transformation on
the trajectories is expected to be insignificant in these cases.   Furthermore, it is believed
that the CFL criterion in the polar region was virtually satisfied in the NIPR model,

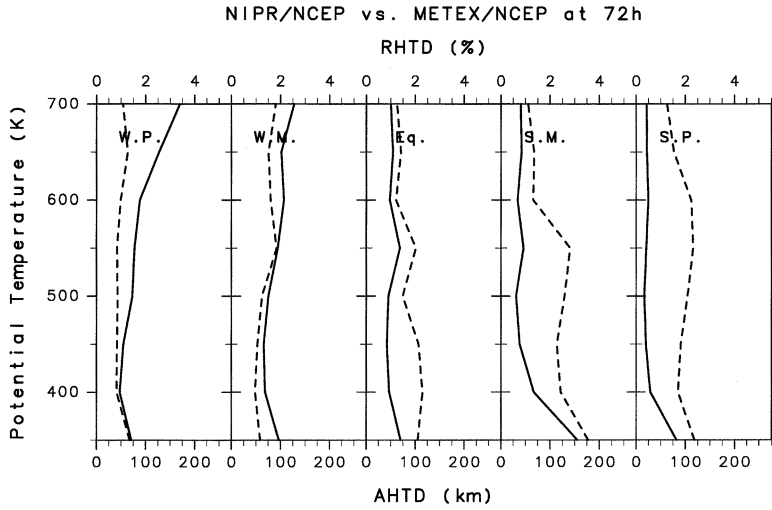NIPR/NCEP vs. METEX/NCEP at 72h

RHTD (%)

Fig. 6.   The same as Fig. 4 but for isentropic trajectories as a function of potential temperature.
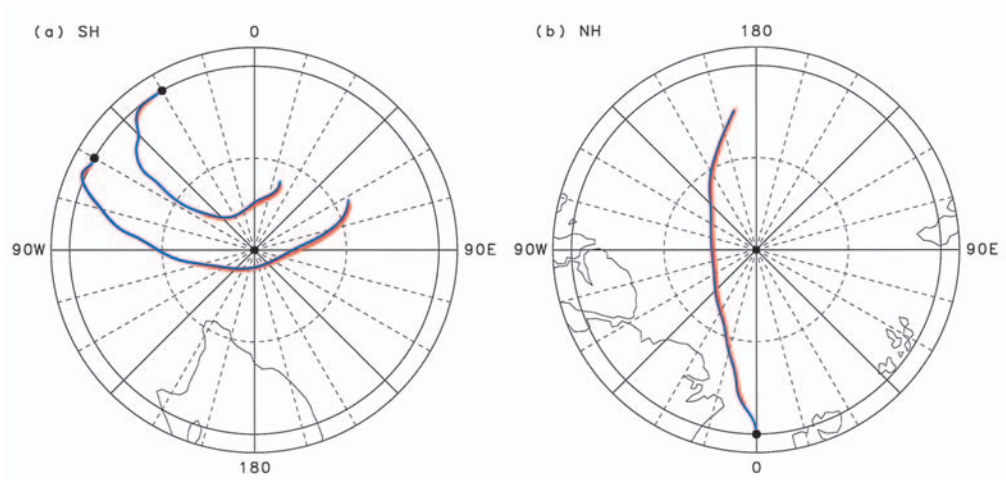

Fig. 7.   Isentropic trajectories at 500 K, which passed (a) south of 87.5°S and (b) north of 87.5°N.
Blue and red lines represent the trajectories calculated with the NIPR model and METEX,
respectively. Solid circles show the initial positions. Solid and dashed latitude lines rep-
resent 80° and 85° latitudes, respectively.

because the forecast model used for operational analysis employs spherical harmonics
and its horizontal resolution is uniform throughout the sphere.

4.2.   NIPR/NCEP vs. NIPR/ECMWF

Figure 8 shows the AHTDs and RHTDs at 72 h for kinematic trajectories resulting
from NIPR/NCEP *vs.* NIPR/ECMWF in five latitude regions as a function of initial
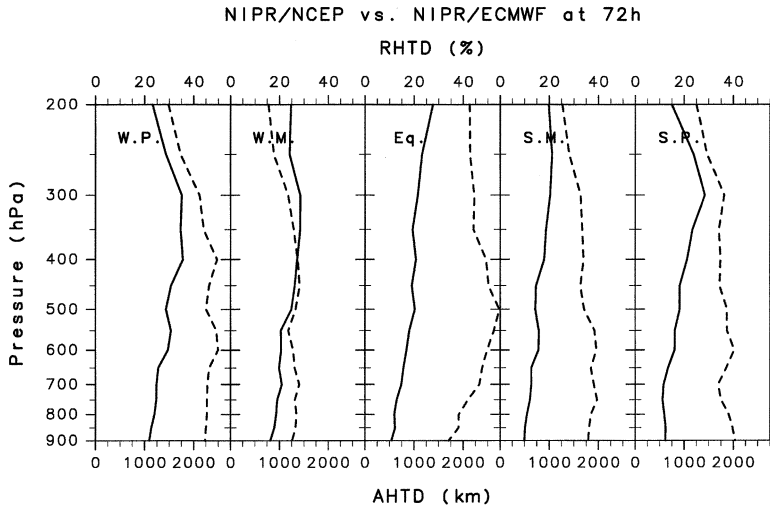pressure.   Although both the AHTDs and RHTDs exhibit some dependence on initial

NIPR/NCEP vs. NIPR/ECMWF at 72h

RHTD (%)

Fig. 8.   The same as Fig. 4 but for NIPR/NCEP vs. NIPR/ECMWF.

NIPR/NCEP vs. NIPR/ECMWF at 72h
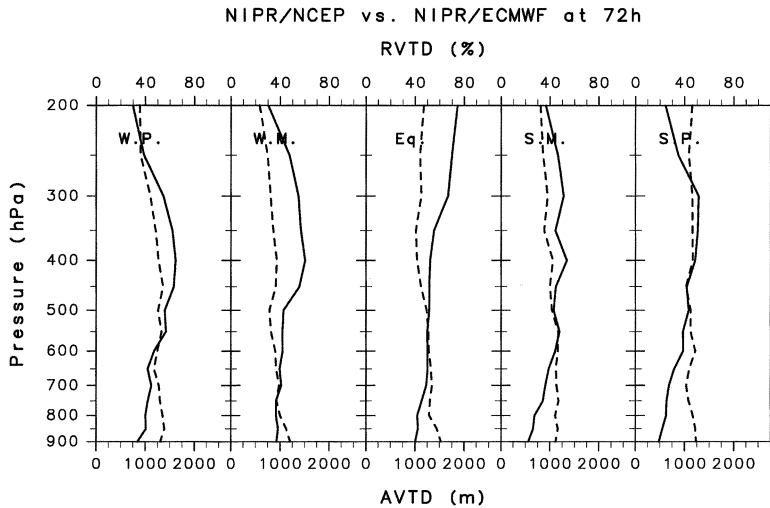
RVTD (%)

Fig. 9.   The same as Fig. 5 but for NIPR/NCEP vs. NIPR/ECMWF.

pressure and latitude as in the case of NIPR/NCEP *vs.* METEX/NCEP, the values of AHTDs and RHTDs for NIPR/NCEP *vs.* NIPR/ECMWF are much larger than those for NIPR/NCEP *vs.* METEX/NCEP.   The AHTDs and RHTDs for NIPR/NCEP *vs.* NIPR/ECMWF are about 1000 km and 40%, respectively, 5–10 times larger than those for NIPR/NCEP *vs.* METEX/NCEP.   These values of RHTDs are comparable to or smaller than those obtained in Pickering *et al.* (1996), which computed the RHTDs at 120 h in the South Atlantic from the National Meteorological Center (NMC) and ECMWF analysis data.   The AVTDs and RVTDs for the kinematic trajectories shown
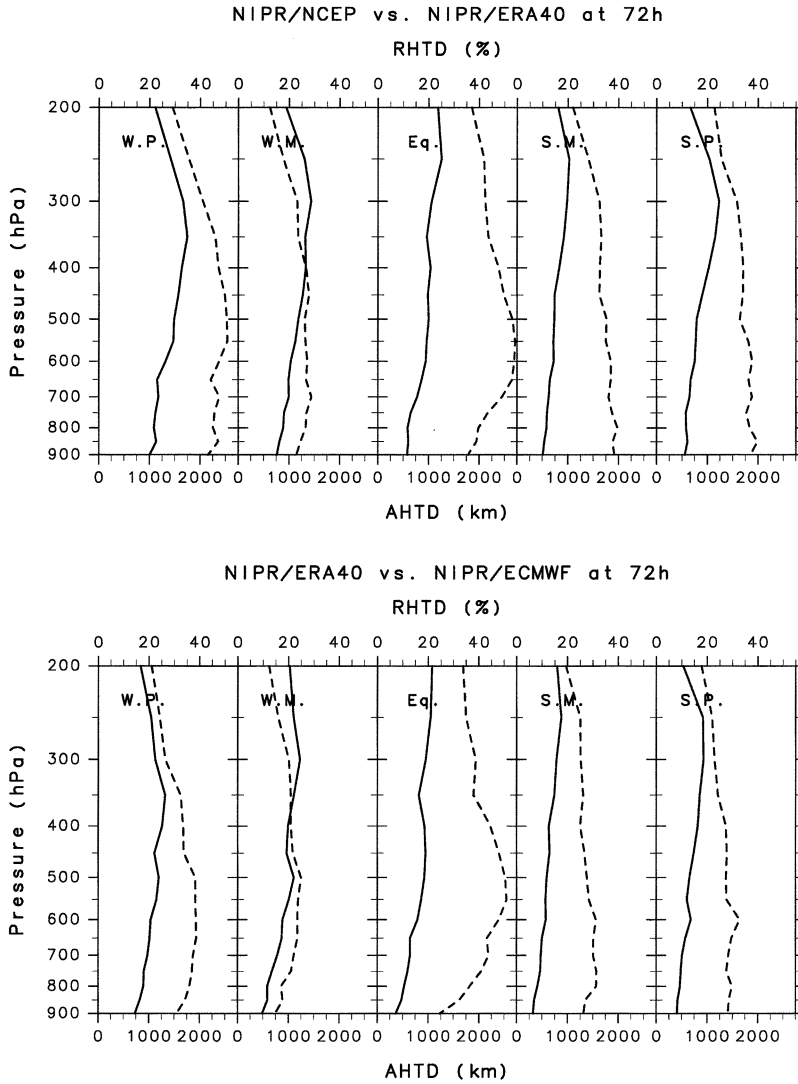
NIPR/NCEP vs. NIPR/ERA40 at 72h

RHTD (%)

AHTD (km)

NIPR/ERA40 vs. NIPR/ECMWF at 72h

RHTD (%)

AHTD (km)

Fig. 10.   *The same as Fig. 4 but for (top) NIPR/NCEP vs. NIPR/ERA40 and (bottom) NIPR/*
           ERA40 vs. NIPR/ECMWF.

in Fig. 9 and the AHTDs and RHTDs for isentropic trajectories (not shown) also have
values 5–10 times larger than those for NIPR/NCEP *vs.* METEX/NCEP.   This fea-
ture does not change even at 24 and 48 h.
    Figure 10 shows the AHTDs and RHTDs at 72 h for kinematic trajectories re-
sulting from NIPR/NCEP *vs.* NIPR/ERA40 and NIPR/ERA40 *vs.* NIPR/ECMWF in
five latitude regions as a function of initial pressure.   In spite of the fact that the same
forecast model is employed for the construction of the ECMWF and ERA40 data, the
AHTDs and RHTDs for NIPR/ECMWF *vs.* NIPR/ERA40 are of the same order as

Table 3. Root mean square differences of U, V, and W at
          500 hPa between NCEP/NCAR Reanalysis 1,
          ECMWF operational analysis, and ECMWF 40-
          year Re-analysis data.

	U (m s^{-1})	V (m s^{-1})	W (Pa s^{-1})
NCEP-ECMWF	4.46	4.02	0.127
NCEP-ERA40	3.74	3.54	0.117
ECMWF-ERA40	3.61	3.03	0.122

those for the other combinations.   Table 3 gives the root mean square (RMS) differences of zonal, meridional, and vertical wind speeds at 500 hPa among the NCEP, ECMWF, and ERA40 data.   The RMS differences between the ECMWF and ERA40 data are not always smaller than the RMS differences for the other combinations, which would lead to AHTDs and RHTDs of the same order.   It is considered that the differences of model resolution (*i.e.*, T213L31 for operational analysis and T159L60 for reanalysis) and data assimilation method (*i.e.*, 4D-Var for operational analysis and 3D-Var for reanalysis) at ECMWF produced the RMS differences between the ECMWF and ERA40 data.

5.   Summary and concluding remarks

The kinematic and isentropic trajectory models recently developed at NIPR were compared with METEX, developed at CGER/NIES.   The difference in the air parcel positions after 72 h travel time is up to 200 km in the horizontal and 200 m in the vertical for the kinematic trajectories in the troposphere.   The difference in the horizontal position is smaller for the isentropic trajectories than for the kinematic trajectories. The relative difference in the horizontal and vertical positions at 72 h is up to 5% and 10 % of horizontal and vertical travel distances, respectively.   The NIPR model shows good agreement with METEX even in the polar region, where the difference between the NIPR model and METEX in time step and coordinate transformation may cause large discrepancies in the calculated trajectories.

An intercomparison among three different datasets (NCEP, ECMWF, and ERA 40) was also performed using the NIPR trajectory model.   The difference in the horizontal and vertical positions computed with the different datasets is 5–10 times larger than those computed with the different models.   This indicates that the accuracy of the trajectory is far more sensitive to the difference of dataset than to the difference of trajectory model (*i.e.*, time integration scheme, interpolation method, and so on).

The NIPR trajectory model will continue to be upgraded.   Some functions such as the coordinate transformation in the polar region and boundary checking will be added to the model soon.   Furthermore the NIPR trajectory model will support the output of a regional model such as MM5 in the near future.

Acknowledgments

References

Danielsen, E.F. (1968): Stratospheric-tropospheric exchange based on radioactivity, ozone and potential vorticity. J. Atmos. Sci., **25**, 502–518.

Dethof, A., O'Neill, A., Slingo, J.M. and Smit, H.G.J. (1999): A mechanism for moistening the lower stratosphere involving the Asian summer monsoon. Q.J.R. Meteorol. Soc., **125**, 1079–1106.

Dethof, A., O'Neill, A., Slingo, J.M. and Berrisford, P. (2000): Quantification of isentropic water-vapour transport into the lower stratosphere. Q.J.R. Meteorol. Soc., **126**, 1771–1788.

Draxler, R.R. and Hess, G.D. (1997): Description of the HYSPLIT_4 modeling system. NOAA Tech. Memo. ERL ARL-224, 25 p.

European Centre for Medium-Range Weather Forecasts (ECMWF) (2002): Workshop on re-analysis, 5–9 November 2001, Reading, U. K., ERA-40 Proj. Rep. Ser. 3, 443 p.

Fujiwara, M., Tomikawa, Y., Kita, K., Kondo, Y., Komala, N. and other 11 authors (2003): Ozonesonde observations in the Indonesian maritime continent: A case study on ozone rich layer in the equatorial upper troposphere. Atmos. Environ., **37**, 353–362.

Hara, K., Yamagata, S., Yamanouchi, T., Sato, K., Herber, A., Iwasaka, Y., Nagatani, M. and Nakata, H. (2003): Mixing states of individual aerosol particles in spring Arctic troposphere during ASTAR 2000 campaign. J. Geophys. Res., **108** (D7), 4209, 10.1029/2002JD002513.

Hatsushika, H. and Yamazaki, K. (2003): Stratospheric drain over Indonesia and dehydration within the tropical tropopause layer diagnosed by air parcel trajectories. J. Geophys. Res., **108** (D19), 4610, 10.1029/2002JD002986.

Jacob, D.J., Crawford, J.H., Kleb, M.M., Connors, V.S., Bendura, R.J., Raper, J.L., Sachse, G.W., Gille, J. C., Emmons, L. and Heald, C.L. (2003): Transport and Chemical Evolution over the Pacific (TRACE-P) aircraft mission: Design, execution, and first results. J. Geophys. Res., **108** (D20), 9000, 10.1029/2002JD003276.

Kalnay, E., Kanamitsu, M., Kistler, R., Collins, W., Deaven, D. and other 16 authors (1996): The NCEP/ NCAR 40-year reanalysis project. Bull. Am. Meteorol. Soc., **77**, 437–471.

Kida, H. (1983): General circulation of air parcels and transport characteristics derived from a hemispheric GCM Part 2. Very long-term motions of air parcels in the troposphere and stratosphere. J. Meteorol. Soc. Jpn., **61**, 510–523.

Knudsen, B.M. and Carver, G.D. (1994): Accuracy of the isentropic trajectories calculated for the EASOE campaign. Geophys. Res. Lett., **21**, 1199–1202.

Koike, M., Kondo, Y., Kita, K., Takegawa, N., Masui, Y. and other 14 authors (2003): Export of anthropogenic reactive nitrogen and sulfur compounds from the East Asia region in spring. J. Geophys. Res., **108** (D20), 8789, 10.1029/2002JD003284.

Lelieveld, J., Crutzen, P.J., Ramanathan, V., Andreae, M.O., Brenninkmeijer, C.A.M. and other 22 authors (2001): The Indian Ocean Experiment: Widespread air pollution from South and Southeast Asia. Science, **291**, 1031–1036.

Norton, W.A. (1994): Breaking Rossby waves in a model stratosphere diagnosed by a vortex-following

coordinate system and a technique for advecting material contours. J. Atmos. Sci., **51**, 654–673

Oshima, N., Koike, M., Nakamura, H., Kondo, Y., Takegawa, N., Miyazaki, Y., Black, D.R., Shiraki, T., Kita, K., Kawakami, S. and Ogawa, T. (2004): Asian chemical outflow to the Pacific in late spring observed during the PEACE-B aircraft mission. J. Geophys. Res., **109** (D12), 10.1029/2004JD 004976.

Petterssen, S. (1940): Weather Analysis and Forecasting. New York, McGraw-Hill, 221–223.

Pickering, K.E., Thompson, A.M., McNamara, D.P., Schoeberl, M.R., Fuelberg, H.E., Loring Jr., R.O., Watson, M.V., Fakhruzzaman, K. and Bachmeier, A.S. (1996): TRACE A trajectory intercomparison 1. Effects of different input analysis. J. Geophys. Res., **101**, 23909–23925.

Reid, S.J., Rex, M., von der Gathen, P., Fløisand, I., Stordal, F. and other 17 authors (1998): A study of ozone laminae using diabatic trajectories, contour advection and photochemical trajectory model simulations. J. Atmos. Chem., **30**, 187–207.

Rex, M., Salawitch., R.J., Harris, N.R.P., von der Gathen, P., Braathen, G.O. and other 59 authors (2002): Chemical depletion of Arctic ozone in winter 1999/2000. J. Geophys. Res., **107** (D20), 8276, 10.1029/2001JD000533.

Sato, K. and Dunkerton, T.J. (2002): Layered structure associated with low potential vorticity near the tropopause seen in high-resolution radiosondes over Japan. J. Atmos. Sci., **59**, 2782–2800.

Stohl, A. (1999): The Flextra Trajectory Model. University of Munich, Germany, 41 p.

Stohl, A. (2001): A 1-year Lagrangian "climatology" of airstreams in the Northern Hemisphere troposphere and lowermost stratosphere. J. Geophys. Res., **106**, 7263–7279.

Stohl, A., Wotawa, G., Seibert, P. and Kromp-Kolb, H. (1995): Interpolation errors in wind fields as a function of spatial and temporal resolution and their impact on different types of kinematic trajectories. J. Appl. Meteorol., **34**, 2149–2165.

Sutton, R.T., Maclean, H., Swinbank, R., O'Neill, A. and Taylor, F.W. (1994): High-resolution stratospheric tracer fields estimated from satellite observations using Lagrangian trajectory calculations. J. Atmos. Sci., **51**, 2995–3005.

Suzuki, K., Yamanouchi, T., Hirasawa, N. and Yasunari, T. (2004): Seasonal variation of air transport in the Antarctic and atmospheric circulation in 1997. Polar Meteorol. Glaciol., **18**, 96–113.

Terao, Y., Sasano, Y., Nakajima, H., Tanaka, H.L. and Yasunari, T. (2002): Stratospheric ozone loss in the 1996/1997 Arctic winter: Evaluation based on multiple trajectory analysis for double-sounded air parcels by ILAS. J. Geophys. Res., **107**, 10.1029/2001JD000615.

Tomikawa, Y., Sato, K., Kita, K., Fujiwara, M., Yamamori, M. and Sano, T. (2002): Formation of an ozone lamina due to differential advection revealed by intensive observations. J. Geophys. Res., **107**, 10.1029/2001JD000386.

Vaughan, G. and Timmis, C. (1998): Transport of near-tropopause air into the lower midlatitude stratosphere. Q.J.R. Meteorol. Soc., **124**, 1559–1578.

Von der Gathen, P., Rex, M., Harris, N.R.P., Lucic, D., Knudsen, B.M. and other 10 authors (1995): Observational evidence for chemical ozone depletion over the Arctic in the winter 1991–1992. Nature, **375**, 131–134.

Waugh, D.W. and Hall, T.M. (2002): Age of stratospheric air: theory, observations, and models. Rev. Geophys., **40**, 10.1029/2000RG000101.

Waugh, D.W. and Plumb, R.A. (1994): Contour advection with surgery: A technique for investigating finescale structure in tracer transport. J. Atmos. Sci., **51**, 530–540.

Yamanouchi, T., Treffeisen, R., Herber, A., Shiobara, M., Yamagata, S. and other 11 authors (2005): Arctic Study of Tropospheric Aerosol and Radiation (ASTAR) 2000: Arctic haze case study. Tellus B, **57**, 141–152.

Zeng, J., Katsumoto, M., Ide, R., Inagaki, M., Mukai, H. and Fujinuma, Y. (2003): Development of meteorological data explorer for Windows. Data Analysis and Graphic Display System for Atmospheric Research using PC, ed. by Y. Fujinuma, CGER-M014-2003, Center for Global Environmental Research, NIES, 19–73.

Appendix

The coordinate transformation between longitude-latitude (λ, ϕ) and Cartesian coordinates in a region centered at the pole (X, Y) is given by

$$X = a \cos \phi \cos \lambda, \tag{A1}$$

$$Y = a \cos \phi \sin \lambda, \tag{A2}$$

where a is the earth's radius. The case of the North Pole is considered here for simplicity. Using zonal and meridional winds (u, v), the horizontal wind components (U, V) in Cartesian coordinates centered at the North Pole are written as:

$$U = -u \sin \lambda - v \cos \lambda, \tag{A3}$$

$$V = u \cos \lambda - v \sin \lambda. \tag{A4}$$

When an air parcel located at $(\lambda_0, \phi_0, X_0, Y_0)$ at $t=0$ reaches $(\lambda_1, \phi_1, X_1, Y_1)$ in the NIPR model and $(\lambda_2, \phi_2, X_2, Y_2)$ in METEX at $t=\delta t$, we have:

$$\lambda_1 = \lambda_0 + \frac{u}{a \cos \phi} \delta t, \tag{A5}$$

$$\phi_1 = \phi_0 + \frac{v}{a} \delta t, \tag{A6}$$

$$X_2 = a \cos \phi_0 \cos \lambda_0 + U \cdot \delta t, \tag{A7}$$

$$Y_2 = a \cos \phi_0 \sin \lambda_0 + V \cdot \delta t. \tag{A8}$$

When

$$\phi_1 = \phi_0 + \frac{v}{a} \delta t = \frac{\pi}{2} + \delta\phi, \tag{A9}$$

$\pi/2 - \phi_0 \ll 1, |\delta\phi| \ll 1$, and $u=0$ are assumed, giving:

$$
\begin{aligned}
X_1 &= a \cos\left(\frac{\pi}{2} + \delta\phi\right) \cos \lambda_0 \\
&= -a \cos\left(\frac{\pi}{2} - \delta\phi\right) \cos \lambda_0 \\
&= a \cos\left(\frac{\pi}{2} - \delta\phi\right) \cos(\pi + \lambda_0) \\
&\approx a \cdot \delta\phi \cdot \cos(\pi + \lambda_0),
\end{aligned} \tag{A10}
$$

$$Y_1 \approx a \cdot \delta\phi \cdot \sin(\pi + \lambda_0), \tag{A11}$$

$$
\begin{aligned}
X_2 &= \cos \lambda_0 (a \cos \phi_0 - v \cdot \delta t) \\
&\approx -\cos(\pi + \lambda_0)\left\{ a\left(\frac{\pi}{2} - \phi_0\right) - v \cdot \delta t \right\} \\
&= a \cdot \delta\phi \cdot \cos(\pi + \lambda_0),
\end{aligned} \tag{A12}
$$

$$Y_2 \approx a \cdot \delta\phi \cdot \sin(\pi + \lambda_0). \tag{A13}$$

Thus in case of $u=0$, the NIPR method in which the latitude is turned back and the longitude is rotated by $180°$ at the pole is almost equivalent to the method of METEX in which the coordinate transformation is performed.

However, in case of $u \neq 0$, since the second term on the right-hand side of (A5) is divergent at the pole, where $\cos \phi \rightarrow 0$, λ_1 is highly variable there. Figure A1 shows the latitude difference, longitude difference, and distance between $(\lambda_1, \phi_1, X_1, Y_1)$ and $(\lambda_2, \phi_2, X_2, Y_2)$ as a function of zonal wind and ϕ_0 for $v = 10\,\mathrm{m\,s^{-1}}$. All three differences increase as the zonal wind speed increases and ϕ_0 approaches the pole. All the differences do not look smooth at $\phi_0 = 89.8°$ because the turnback of latitude at the pole is performed in the NIPR model at $\phi_0 = 89.9°$.
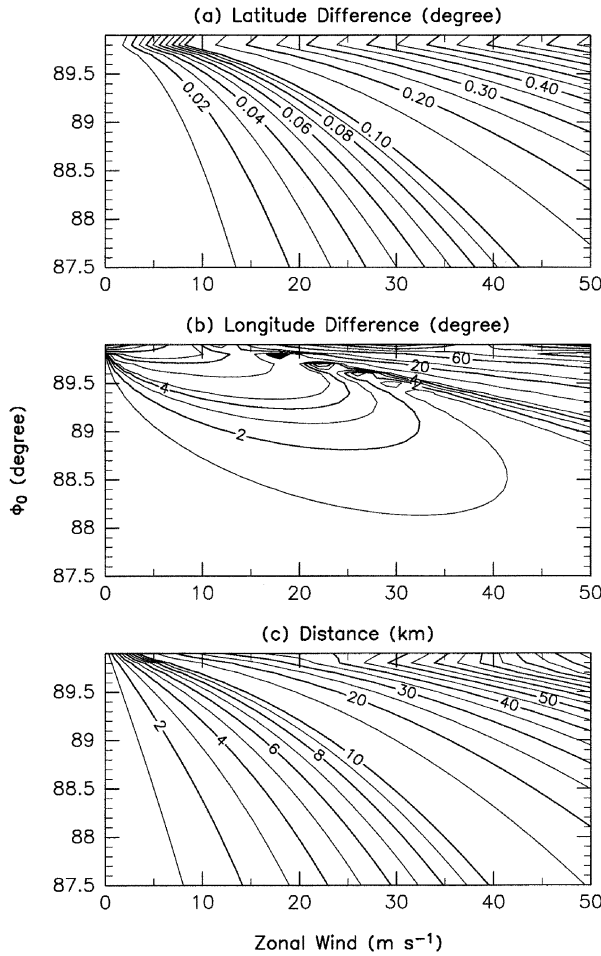

Fig. A1. (a) Latitude difference (degrees), (b) longitude difference (degrees), and (c) distance (km) between $(\lambda_1, \phi_1, X_1, Y_1)$ and $(\lambda_2, \phi_2, X_2, Y_2)$ as a function of zonal wind (m s^{-1}) and ϕ_0 (degrees) for $v = 10\,m\,s^{-1}$.